https://doi.org/10.22226/2410-3535-2022-4-399-403

New low-activation austenitic steel for nuclear power engineering

I. Yu. Litovchenko[†,1], S. A. Akkuzin[1], N. A. Polekhina[1], K. V. Almaeva[1],
E. N. Moskvichev[1], A. V. Kim[1], V. V. Linnik[1], V. M. Chernov[2]
[†]litovchenko@ispms.ru

[1]Institute of Strength Physics and Materials Science of the Siberian Branch of the RAS, Tomsk, 634055, Russia
[2]A. A. Bochvar High-Technology Research Institute of Inorganic Materials, Moscow, 123098, Russia

Vacuum induction melting is used to fabricate a new low-activation chromium-manganese austenitic steel with an increased, compared to well-known analogues, manganese content and additional alloying with strong carbide-forming elements (with a high tendency to carbide formation). Using the methods of transmission and scanning electron microscopy, the features of its microstructure, elemental and phase compositions in the solution treated state are studied. It is shown that the steel has an austenitic structure with a grain size of tens of micrometers. Its dislocation substructure is represented by flat dislocation pileups, which is typical for materials with low stacking fault energy. Coarse (submicron) particles of MC carbides (M = Ti, Ta, Zr, W) are found along the boundaries and inside the grains. Nanosized particles of the MC type fix the grain and subgrain boundaries and the dislocation substructure of the steel. Mechanical tensile tests are carried out at room and elevated temperatures. It is shown that the new steel has higher yield and tensile strength values, as well as elongation to failure compared to the austenitic chromium-nickel steels currently used in nuclear power engineering and well-known chromium-manganese low-activation steels.

Keywords: low-activation materials, austenitic steels, microstructure, strength, plasticity.

1. Introduction

Currently, the most common structural materials in nuclear power engineering, in particular the materials of the nuclear reactor fuel elements, are chromium-nickel austenitic steels [1–5]. They have a number of attractive properties, such as high heat resistance, increased resistance to radiation embrittlement and advanced corrosion resistance. However, at high radiation doses (more than 100 dpa), the austenitic chromium-nickel steels exhibit a tendency to radiation swelling. It should be noted that these steels, due to the high nickel content after irradiation, exhibit a slow drop of induced radioactivity, which contributes to the accumulation of unwanted radioactive material waste. Moreover, in the EK-164 (Fe-16Cr-19Ni-2Mo-2Mn-Nb-Ti-B) austenitic steels and their foreign analogues [1,2,5], currently used in Generation III reactors, the nickel (highly activation element) content has been increased to 15–19%. Despite the unsolvable problem of high radiation accumulation capability, these steels are thought to be possible candidates for the structural materials of Generation IV reactors [1–5].

The 9–12% Cr ferritic-martensitic steels have been proposed as an alternative to chromium-nickel austenitic steels [1–9]. In contrast to austenitic steels, they have a much lower tendency to radiation swelling. Their main problems are insufficient values of heat resistance and a tendency to low-temperature embrittlement, which is largely manifested under irradiation conditions. Earlier we showed [8–10] a possibility of increasing the short-term high-temperature strength of ferritic-martensitic steels by increasing the efficiency of dispersion and substructural strengthening. It was demonstrated that the low-activation ferritic-martensitic steel EK-181 (Fe-12Cr-2W-V-Ta-B) has high short-term strength properties at 650°C and thermal stability of microstructure and mechanical properties under conditions of prolonged (13 500 h.) high-temperature aging at 620°C [9].

Despite the fact that new low-activation alloys and steels have been developed by now and are being actively investigated, higher operating temperatures and degrees of the nuclear fuel burnout and a planned reduction in the environmental load from the nuclear waste structural materials necessitate the search for new compositions and the development of new alloys that would meet these conditions. The design of new low-activation austenitic steels as a new research avenue was initiated in [5,11,12] — Russia, [13] — USA and [14,15] — Japan in the 90s of the XX century and in early 2000s. In these works on the Fe-12Cr-(20–25) Mn alloys, it is shown that such steels with a carbon content of 0.1–0.25 wt.% have an austenitic structure with coarse particles of $M_{23}C_6$ carbides along the grain boundaries and MC particles in the grain interior. The reduced carbon and manganese content contributes to a decrease in the stability of the austenite undergoing γ-ε and γ-ε-α' transformations under plastic deformation. The presence of martensitic phases in the steel structure is unfavorable for the behavior of steels under irradiation conditions, since it can cause additional swelling [13].

Despite the high interest in low-activation austenitic steels and a significant number of relevant publications within the above-mentioned period [5,11–15], the research of low-activation ferritic-martensitic steels has become even more extensive [1–9]. In recent years, there have been only

few publications on the study of microstructure, mechanical and corrosion properties of low-activation austenitic steels [16,17]. Meanwhile, based on theoretical calculations of nuclear-physical characteristics, it was shown [18] that these steels could have a reduced tendency to high-temperature embrittlement and helium production under irradiation conditions than that of the chromium-nickel steels (EK-164 type). Potentially low-activation austenitic Cr-Mn steels are of particular interest for thermonuclear reactors with magnetic plasma confinement (tokamak-type), in which application of nonmagnetic steels as structural materials is an important advantage [18]. The issues of high-temperature embrittlement and radiation swelling of such materials require additional studies. Moreover, according to the literature data [13], the radiation swelling of stable chromium-manganese austenite is lower than that of metastable austenite. Therefore, research is needed to develop and study new compositions of stable steels of this class. The purpose of this work is to develop a new composition of a low-activation chromium-manganese austenitic steel with an increased austenite stability, effectively using dispersion and substructural strengthening, to manufacture it and to provide a primary validation of its microstructure and mechanical properties.

2. Materials and experimental method

The steel of a new composition of Fe-29Mn-12Cr-W-Si-Ta-Ti-V-Zr-0.25C, wt.% was melted in a vacuum induction furnace. The weight of the experimental ingot is 2.5 kg. A significant difference from the previously studied compositions [5,11–15] is a higher content of manganese and an increased content of strong carbide-forming elements (with a high tendency to carbide formation): Ta, Ti, V, Zr, W. In accordance with the concept of low-activation materials, the content of such highly activated elements as Ni, Cu, Nb, Mo, Co, Al in the new steel, also N and O is reduced to the minimum level.

The elemental composition of the new steel was studied by various methods in a Shimadzu XRF-1800 X-ray fluorescence spectrometer, in an ISKROLINE 300K optical emission spectrometer, and using an Octane Elect Super (EDAX) X-ray microanalysis attachment to an Apreo 2 S Scanning Electron Microscope (Thermo Fisher Scientific).

After melting, the ingot was homogenized at 1100°C for 2 hours. After homogenization, it was hot forged at 1100°C, followed by a solution treatment (ST) at 1100°C for 1 hour and subsequent air cooling. The features of its microstructure, elemental and phase compositions were studied in the ST state.

Metallographic studies were carried out in an AXIOVERT-200MAT microscope (Zeiss, Germany). The surface for optical studies was polished electrolytically.

The microstructural characterization was performed using an Apreo 2 S Scanning Electron Microscope (SEM) equipped with a Field Emission Gun (FEG) and a Velocity-Super (EDAX) Electron Backscatter Diffraction (EBSD) detector. The SEM samples were prepared by mechanical polishing followed by ion milling as a final polishing step. Ion polishing was performed using a Technoorg Linda SEMPrep 2 system. The EBSD data were obtained with step sizes of 2 μm for the area of 1 mm^2. The microstructure was examined by the EDAX OIM software.

Transmission Electron Microscopy (TEM) investigations were conducted using a JEOL JEM-2100 electron microscope at an accelerating voltage of 200 kV in TEM and Scanning Transmission Electron Microscopy (STEM) mode. Thin foils were prepared by electropolishing in an electrolyte containing 450 ml of orthophosphoric acid and 50 g of chromic anhydride.

Mechanical tests were carried out by the method of static tensile deformation at a strain rate of $\approx 2\times10^{-3}$ s^{-1} at room temperature (20°C) on a MIM 2-50 testing machine (Russia) and at high temperature close to the maximum nuclear reactor operating temperature (650°C) on a PV-3012M high-temperature vacuum testing machine (Russia) using dog-bone samples with the gage length of 13 mm and the gage section of 2×1 mm^2. High temperature tensile tests were carried out in a vacuum of $\approx 2.5 - 3.5\times10^{-5}$ Pa.

3. Results and discussion

The average values of the element content in the new steel determined by the above methods are presented in Table 1.

From the analysis of Table 1, it follows that the resulting ingot is indeed a low-activation material, since it contains the minimum values of such high-activation elements as Ni, Cu, Nb, Mo, Co, and no such elements as Al, N, O were found.

Metallographic studies (Fig. 1a) showed that the boundaries of almost equiaxed austenite grains and coarse particles had been etched on the surface. The etching of austenite grain boundaries in the polishing mode is apparently due to the presence of second-phase particles at them. SEM studies confirm this (Fig. 1b). Coarse (submicron and micron) precipitates are observed in the body of the grains and along the grain boundaries. The data of the elemental analysis of several particles, indicated in (Fig. 1b), and the matrix are presented in Table 2. This analysis suggests that the particles indicated above are the Ti, Ta and Zr enriched carbides.

SEM EBSD studies (Fig. 2) showed that in the ST state the new steel is characterized by austenitic grains with an average size of 50 μm. The grain boundary maps clearly show that, in addition to high-angle boundaries, there are a significant number of twin boundaries, which are apparently the annealing twins. One should also note an increased number of low-angle boundaries (dislocation substructures); their formation could have been caused by quenching stresses developing near coarse carbide particles. No phases other than the austenite were detected by the SEM EBSD method.

TEM studies of the features of the heterophase and defect microstructure of the new steel showed the presence of planar dislocation substructures with coarse and fine particles (Fig. 3 a) and multiple stacking faults (Fig. 3 b). In

Table 1. Elemental composition of the ingot of a new low-activation chromium-manganese austenitic steel, Fe — base, wt.%.

Cr	Mn	Ni	Cu	W	V	Ti	Ta	Zr	Nb	Mo	Co	Si	S	P	C	B
11.9	28.7	0.06	0.08	0.9	0.4	0.11	0.2	0.03	0.01	<0.01	0.02	0.5	0.013	<0.01	0.26	0.004

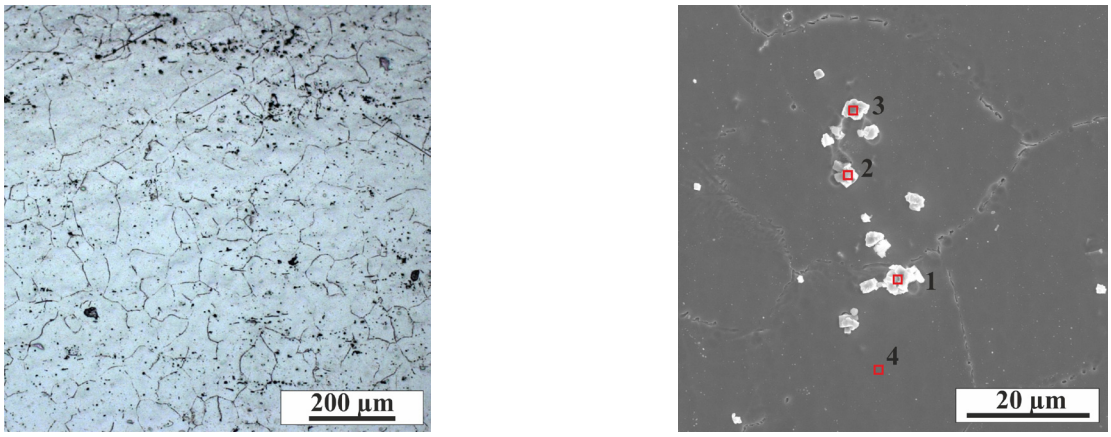

a b

Fig. 1. (Color online) Grain structure of steel. Optical image (a), SEM image with marked up EDS spots (b).

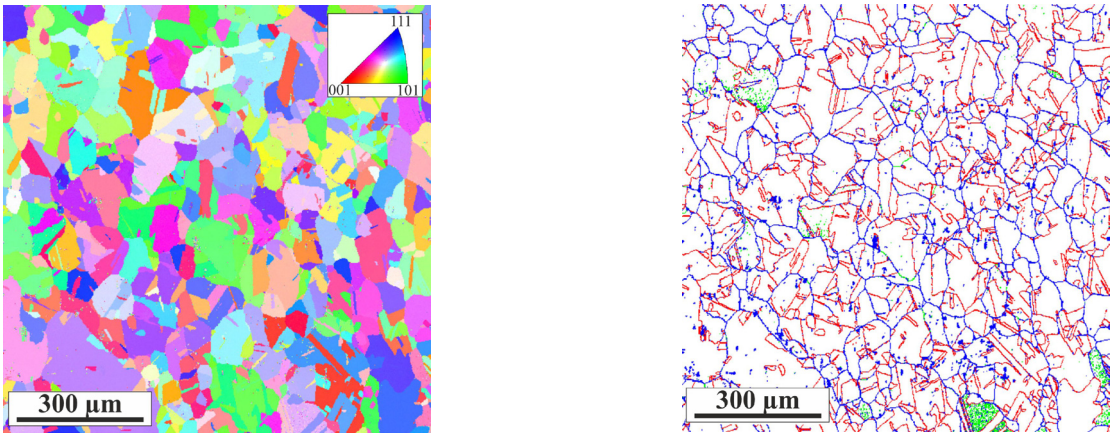

a b

Fig. 2. (Color online) SEM EBSD images of steel structure. Orientation map (a), grain boundary map with high-angle, twin and low-angle boundaries indicated by blue, red and green color, respectively (b).

Table 2. Elemental analysis data for the points marked in Fig. 1.

Element	Wt.%			
	1	2	3	4
Si	0.0	0.0	0.0	0.80
Ti	40.9	6.60	50.7	0.1
V	2.5	0.4	2.9	0.3
Cr	2.9	1.7	2.6	11.16
Mn	2.8	3.9	1.9	30.2
Fe	3.4	5.9	2.6	53.1
Zr	21.0	78.1	22.7	0.1
Ce	14.3	0.6	2.3	1.0
Ta	12.2	2.8	14.4	2.7
Total	100.00	100.00	100.00	100.00

this case, similarly to the numerous dispersion strengthened steels, nanosized particles pin the dislocation substructure. In the process of TEM studies, no bcc phase (α-ferrite), σ-phase, or carbides of the $M_{23}C_6$ type, which can be formed in chromium-manganese austenitic steels [11,12], were found.

Element mapping of the region near one of the dispersed particles is shown in Fig. 4. It implies that this particle with a diameter of about 150 nm might be a complex carbide alloy of the MC type mainly enriched in Ti, V, Ta, W, Zr and Si.

In addition to multiple stacking faults, the low stacking fault energy of the investigated new austenitic steel is evidenced by the tendency towards forming mechanical twins. Twins in several twinning systems are easily formed in the stressed regions near the thin foil edge. Figure 5 shows a characteristic bright-field image of the microtwin plates and the corresponding diffraction pattern in which twin reflections can be observed.

According to the estimates in the JMatPro program [19], the stacking fault energy for the composition presented in Table 1 at room temperature is 25 mJ/m^2. The low SFE is in a good agreement with the above microstructure features.

Tensile curves for new steel at 20 and 650°C are shown in Fig. 6. At elevated tensile temperature (650°C) regions with serrated plastic flow were found in the curve 2. These features of the curve are associated with the dynamic strain aging. Table 3 presents the average values of the yield strength, tensile strength and elongation to failure for new steel and the corresponding values of the mechanical properties of other reactor steels, taken from [12,21]. A comparison of these properties with the corresponding mechanical properties of the chromium-nickel austenitic steel EK-164 [20,21], currently used in nuclear power engineering, and the properties of the low-activation chromium-manganese austenitic steels of the 12Cr-20Mn type [11,12], demonstrates the advantages of the new steel (Table 3). Its higher values of the room-temperature strength properties are apparently due to the increased dislocation density and the higher

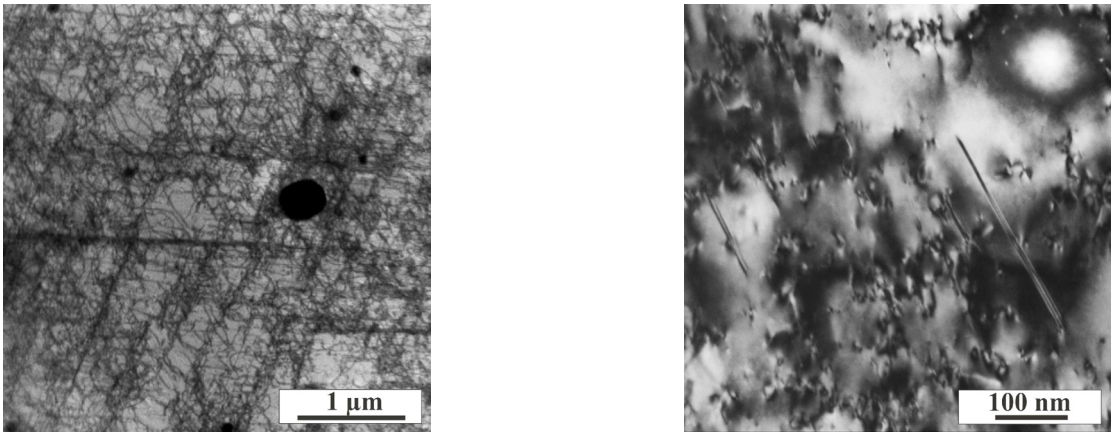

a b

Fig. 3. TEM images of steel microstructure. Bright Field (BF) scanning transmission electron microscopy (STEM) image of dislocation substructure and dispersed particles (a), BF TEM image of stacking faults and dislocation substructure (b).

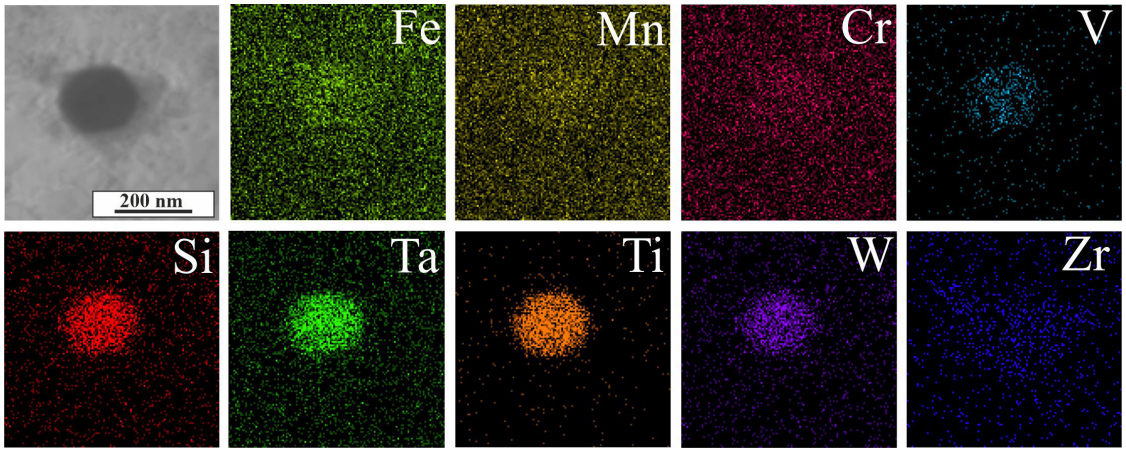

Fig. 4. (Color online) STEM BF image and elemental map of the region near the dispersed particle.

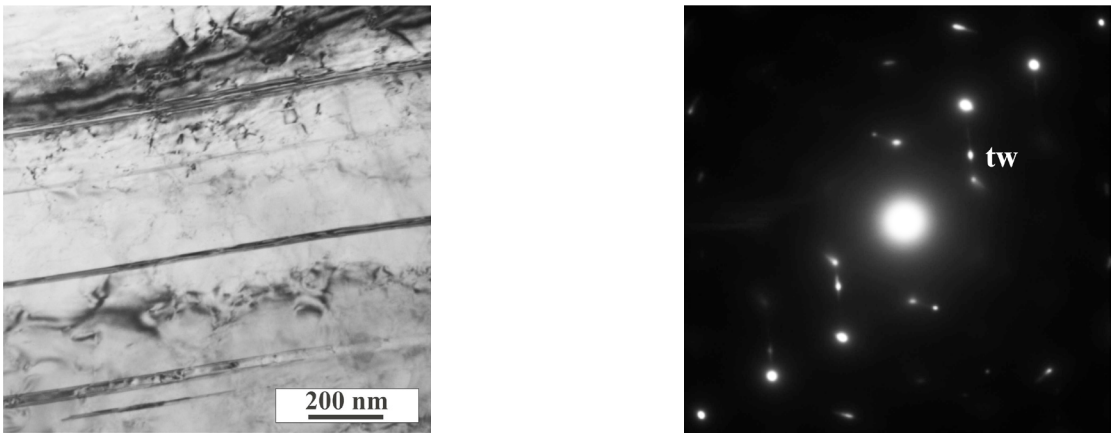

a b

Fig. 5. TEM image of steel microstructure. BF image (a), selected area diffraction pattern (b), zone axis close to [110].

Table 3. Comparison of mechanical properties of reactor austenitic steels.

Material	Tensile tests temperature, °C	Yield strength, MPa	Tensile strength, MPa	Elongation to failure, %
Fe-29Mn-12Cr-1.4W-Si-Ta-Ti-V-Zr-0.25C	20	311±21	662±76	79.2±3.5
	650	95±10	353±63	42.4±4.2
Fe-17.9Ni-15.9Cr-2.4Mo-1.7Mn-Si-Ti-Nb-V-0.07C [21]	20	201±2	539±10	47.4±0.1
	650	95±6	360±9	31±1.6
Fe-20Mn-12-Cr-W-0.25C [12]	20	249	687	50.2
	600	115	318	38.9

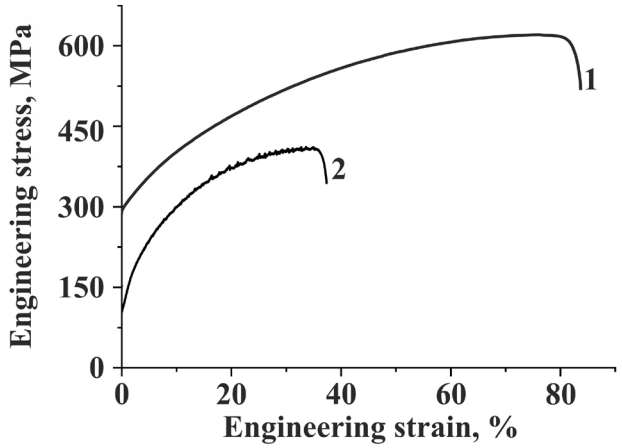

Fig. 6. Engineering stress - engineering strain curves of some treated steel samples: 1 — tension at 20°C, 2 — tension at 650°C.

density of dispersed carbide particles that pin the dislocation substructure. Higher values of plasticity are associated with the low stacking fault energy and the twinning induced plasticity (TWIP) effect during deformation, and possibly the transformation induced plasticity (TRIP) effect during the γ-ε martensitic transformation, which is characteristic of the austenitic steels having a high content of manganese [11–15].

4. Conclusions

A new low-activation chromium-manganese austenitic steel with an increased manganese content, compared to well-known analogues, and additional alloying with strong carbide formers has been melted. The features of the microstructure, elemental and phase composition of the new steel in the state after solid solution treatment have been studied. It has been shown that the steel has a single-phase austenitic structure with coarse and fine particles of carbide phases enriched in Ti, Ta, and Zr. It is characterized by the formation of planar dislocation substructures, stacking faults, and a tendency to mechanical twinning, which is due to the low stacking fault energy. The new steel has higher strength and plastic properties at room temperature compared to the known analogues, which is due to the increased dispersion and substructural strengthening and the TWIP effect during plastic deformation.

Acknowledgements. The study was funded by a grant of the Russian Science Foundation Project No. 22-19-00802 https://rscf.ru/project/22-19-00802/. The research was done using equipment of Tomsk Regional Core Shared Research Facilities Centre of National Research Tomsk State University and the Share Use Centre "Nanotech" of the Institute of Strength Physics and Materials Science SB RAS.

References

1. Y. Pascal. Structural Materials for Generation IV Nuclear Reactors. Woodhead Publishing Series in Energy: Number 106, Kindle Edition (2020) 644 p.
2. G. S. Was, D. Petti, S. Ukai, S. Zinkle, J. Nucl. Mater. 527, 151837 (2019). Crossref
3. F. A. Garner. Comprehensive Nuclear Materials. 2nd edition. 3, 57 (2020). Crossref
4. R. G. Odette, S. J. Zinkle. Structural Alloys for Nuclear Energy Applications. Elsevier (2019) 655 p.
5. L. I. Ivanov, Yu. M. Platov. Radiation physics of metals and its applications. Moscow, Interkontakt Nauka (2002) 300 p. (in Russian)
6. V. M. Chernov, M. V. Leonteva-Smirnova, M. M. Potapenko, et. al. Nucl. Fusion. 47, 839 (2007). Crossref
7. R. L. Klueh, N. Hashimoto, P. J. Maziasz. J. Nucl. Mater. 367, 48 (2007). Crossref
8. N. A. Polekhina, I. Yu. Litovchenko, A. N. Tyumentsev, D. A. Kravchenko, V. M. Chernov, M. V. Leontyeva-Smirnova. Tech. Phys. 62 (5), 736 (2017). Crossref
9. N. A. Polekhina, I. Yu. Litovchenko, K. V. Almaeva, A. N. Tyumentsev, V. M. Chernov, M. V. Leontyeva-Smirnova. Inorg. Mater.: Applied Research. 13 (5), 1247 (2022). Crossref
10. I. Litovchenko, K. Almaeva, N. Polekhina, S. Akkuzin, V. Linnik, E. Moskvichev, V. Chernov, M. Leontyeva-Smirnova. Met. 12, 79 (2022). Crossref
11. E. V. Demina, M. D. Prusakova, V. V. Roshchin, N. A. Vinogradova, G. D. Orlova. Inorg. Mater.: Applied Research. 1, 115 (2010). Crossref
12. E. V. Demina, L. I. Ivanov, Yu. M. Platov, M. D. Prusakova, S. R. Eikholtser, M. B. Tolochko, F. A. Garner. Inorg. Mater.: Applied Research. 2, 457 (2011). Crossref
13. R. L. Klueh, P. J. Maziasz. Mater. Sci. Eng., A. 127, 17 (1990). Crossref
14. M. Onozuka, T. Saida, Sh. Hirai, M. Kusuhashi, I. Sato, T. Hatakeyama. J. Nucl. Mater. 255, 128 (1998). Crossref
15. Y. Suzuki, T. Saida, F. Kudough. J. of Nucl. Mater. 258, 1687 (1998). Crossref
16. M. M. Eissa, S. U. El-kameesy, S. A. El-Fiki, S. N. Ghali, R. M. El Shazlyc, A. Saeed. Fusion Eng. Des. 112, 130 (2016). Crossref
17. A. Saeed, R. M. El-Shazly, S. N. Ghali, S. Y. El-khamisy, S. A. El-Moneem El-fiki, M. M. Eissa. Nucl. Sci. 3, 45 (2018). Crossref
18. A. I. Blokhin, V. M. Chernov. Physics of Atomic Nuclei. 84 (7), 1272 (2021). Crossref
19. JMatPro. Practical software for materials properties: Website (accessed on 2001)
20. S. A. Akkuzin, I. Yu. Litovchenko, A. N. Tyumentsev, V. M. Chernov. Rus. Phys. Journal. 62, 698 (2019). Crossref
21. S. Akkuzin, I. Litovchenko, N. Polekhina, K. Almaeva, A. Kim, E. Moskvichev, V. Chernov. Metals. 12, 63 (2022). Crossref